Proceedings of the ASME 2022
International Design Engineering Technical Conferences Computers and Information in Engineering Conference
IDETC 2022
August 14–August 17, 2022, St. Louis, Missouri

IDETC2022-91303

A SELF-REACTIVE OCEAN WAVE ENERGY CONVERTER WITH WINCH-BASED POWER TAKE-OFF: DESIGN, PROTOTYPE, AND EXPERIMENTAL EVALUATION

Mingyi Liu[1], Adam Bennett[2], Fujun Ruan[1], Xiaofan Li[1], Junhui Lou[2], Jia Mi[1], Lei Zuo[1,*]

[1]Department of Mechanical Engineering, Virginia Tech, Blacksburg, VA, U.S.A.
[2]E-Wave Technologies LLC, Poughkeepsie, NY, U.S.A.

ABSTRACT

Agriculture provides a large amount of the world's fish supply. Remote ocean farms need electric power, but most of them are not covered by the electric power grid. Ocean wave energy has the potential to provide power and enable fully autonomous farms. However, the lack of solid mounting structure makes it very challenging to harvest ocean power efficiently; the small-scale application makes high-efficiency conversion hard to achieve. To address these issues, we proposed a self-reactive ocean wave converter (WEC) and winch-based Power Take-Off (PTO) to enable a decent capture width ratio (CWR) and high power conversion efficiency. Two flaps are installed on a fish feed buoy and can move along linear guides. Ocean wave in both heave and surge directions drive the flaps to move and hence both wave potential energy and wave kinetic energy are harvested. The motion is transmitted by a winch to rotation motion to drive an electric generator, and power is harvested. Dynamic modeling is done by considering the harvester structure, the added mass, the damping, and the excitation force from ocean wave. The proposed WEC is simulated in ANSYS AQWA with excitations from regular wave and results in a gross CWR of 13%. A 1:3.5 scaled-down PTO is designed and prototyped. Bench-top experiment with Instron is done and the results show that the mechanical efficiency can reach up to 83% and has potential for real applications.

Keywords: Ocean wave energy, Self-reaction, Power take-off, Efficiency, Winch-based

1. INTRODUCTION

According to the United Nations Food and Agriculture Organization (FAO) wild fisheries are heavily depleted and many ocean ecosystems are at risk of collapse due to a variety of ecological disasters [1]. The fishing industry has been forced to turn to an alternative means of production. The production that has answered this demand is called aquaculture and by 2014 it had grown to 45% of the world's fish market share [2]. This growth is projected to only continue and as world population grows the increased demand of fish production will continue to fall on aquaculture, not wild capture. By 2020 the global aquaculture market is projected to be more than 55 billion USD according to FAO [2] Aquaculture is the only way in the foreseeable future that can satiate this demand. Modern ocean farms need electric power, however, many of them are not covered by the power grid due to remote locations. It is challenging to provide power supply for remote ocean farm operations and maintenance, which includes sensors, monitors, and fish food distributors. Currently, diesel generator is the typical solution but is expensive and inconvenient due to fuel supply and logistic cost. On the other hand, the ocean embodies a huge amount of energy. According to [3], the power potential on the U.S. coast is 2,640 TWh/year, which is equivalent to 2/3 of the 4,000 TWh/year of the electricity consumed by the whole country. The ocean has the potential to provide a clean, sustainable, and convenient energy supply to ocean farms.

In literature, there are many ocean energy harvesting solutions. The main ocean energy sources include ocean wave and ocean current. Ocean wave energy comes from the potential and kinetic energy of the wave, and has the greatest potential. Ocean Wave Energy Converter (WEC) converts the wave energy to electricity. The mainstream WEC includes point absorber [4], attenuator [5] [6], oscillating wave surge converter [7], oscillating water column [8], overtopping device [9], and submerged pressure differential device [10]. According to the fixture type, the WECs can be categorized into floating type and fixed type. The wave to electrical power conversion efficiency is measured by Capture Wave Ratio (CWR), which is the ratio between electrical power output over the wave energy input rate. Most of the high-efficiency WECs are fixed type. For example, the best conversion efficiency is 72% and achieved by the oscillating wave surge converter [11]. Oscillating water column can also achieve CWR as much as 58% [12]. However, the oscillating water col-

*Corresponding author: leizuo@vt.edu
Documentation for `asmeconf.cls`: Version 1.30, May 17, 2022.

umn devices are costly. Tethered to the button of the ocean floor, the heaving device can achieve an efficiency of 46% [12]. The maximum CWR that can be achieved by the overtopping device is 27% [13].

However, all those devices need a fixed base to mount the energy harvesting device, which is not available in typical ocean farm settings. This leaves the choice to the floating wave energy converters. For the floating point absorber and floating oscillating water column, the power conversion efficiency is limited, and the highest efficiency that is achieved is 25% [14] and 18% [15]. Among the wide variety of floating WECs proposed thus far, raft-type WECs have been proven to have a high CWR and also have good survivability in extreme waves. The relative rotation motion around the hinge is used to drive the electric generator, such that the ocean wave power can be converted to electricity. In 1974, Cockerell designed a raft-type WEC, consisting of a series of rafts hinged together by joints [16]. Another good example of raft-type WEC, the Pelamis has undergone a significant development from concept to commercial installation [17]. The raft-based WEC can convert energy efficiently and is thoroughly studied in literature. However, the change of the hinge angle will change the hydrostatic stiffness, and hence changes the resonance frequencies of the whole system. This will lead to the mismatch between the excitation frequency and the resonance frequency. As a result, the system performance is impaired.

Theoretically, the efficiency of duck-type WEC can reach as much as 90% [18]. However, the total energy conversion efficiency is limited due to PTO efficiency. Most of the current PTOs are hydraulic-based [5] and its efficiency drops drastically once the excitation amplitude does not match the designed values [17]. Small size also limits the hydraulic PTO's efficiency. The hydraulic PTO has oil leaking problem, and will potentially pollute the ocean. It is critical to find a high-efficient and high-reliable solution for the PTO.

To address the low power output and low-efficiency issue, we propose a flap-base energy harvesting system with linear guides and a tether-based PTO that can enable high-efficiency power output. The proposed design is composed of two inclined wave capture flaps that can be retrofitted into existing fish feed-buoy; a winch-based PTO that can drive the generator in unidirectional rotation. The flap attack angle will not change due to the motion and hence the system can stay in resonance with the excitations, regardless of the motion range. Compared with other types of PTO, like the hydraulic, ball screw, and rack-and-pinion-based PTOs, the winch-based PTO system is much simpler, reliable, and cost-effective. With a scaled prototype, we demonstrated the feasibility of a tether-based PTO. The simulation and experiment validate the decent capture ratio and high-efficiency conversion.

The rest of this paper is organized as follows. The design of the winch-based PTO will be presented in detail in Section 2. The modeling and simulation will be introduced in Section 3. The system will be prototyped and experimentally tested in Section 4. Finally, conclusions will be given in Section 5

2. DESIGN OF SELF-REACTIVE WEC AND THE WINCH-BASED PTO

The typical ocean farm is consisted of several pens and a feed buoy, as illustrated in Figure 1. A feed vessel will come and distribute fish food periodically. In order to harvest energy from the ocean wave effectively, a base structure in the ocean is expected to have the WEC mounted on it. However, such structures are typically not possessed by ocean farms. A more viable and cost-effective way is to take advantage of the existing ocean farm structures. It is critical to develope technology that can take advantage of the existing structures with a reduced cost while harvesting a decent amount of power for the ocean farm. The most promising candidate is the feed buoy.

In order to achieve high power output while limit the cost, we proposed a WEC that can be retrofitted into existing fish farm infrastructure and achieve resonance with the excitation wave. The proposed WEC is designed to be retrofitted into the feed buoy of the aquaculture system, as shown in Figure 2-A. The WEC has two floating flaps that are attached to the feed buoy and can move linearly along the linear guides. A tether is connected to the floating flap at one end, and connected to the winch of the PTO at the other. The downward flap rotation will pull the winch to drive the generator and power is harvested. The tether rope will be rewound with the help of a torsional spring, getting it ready for the next wave motion. The energy harvested will be stored in the battery in the fish feed buoy to power the fish farm. It shall also be noted that the proposed flap-type WEC harvests power from both surge and heave ocean wave motion, which is totally different from the oscillating surge WEC (like Resolute Marine Energy Inc) which uses only surge wave. As a result, both wave potential energy and wave kinetic energy are taken advantage of.

Through numerical modeling and design, the WEC flaps can resonate with the dominant wave frequency to maximize power capture. The CAD design of the PTO is shown in Figure 2-B. The working principle is as follows. With the initial position shown as the CAD, the tether is driven by the flap and the motion drives the winch to rotate. The rotation motion is magnified by a gearbox and then drives the generator. The output of the generator is shunt to an electric load and power is harvested. A flywheel can be integrated into the generator shaft to smooth the rotation speed. There is a one-way-clutch between the gearbox and the generator. When the flap rotates towards the end of one driving cycle, a one-way clutch will be disengaged and the winch can be in free rotation in the other direction. As the flap is restoring to its original position, the tether will be loose. The torsional spring rotates and drives the winch and the tether back to their original position. In the end, it is back to its initial position and gets ready for the next cycle.

3. DYNAMIC MODELING AND SIMULATION OF WINCH-BASED PTO

3.1 PTO dynamic modeling

The PTO system lumped model is shown in Figure 3.

As shown in Figure 3, the excitation is input displacement x or velocity $\dot{x}$. The translational motion is converted to rotation motion by the winch to $\omega_w = \frac{\dot{x}}{r}$, where r is the radius of the winch. The rotational motion is magnified by the gearbox and hence the

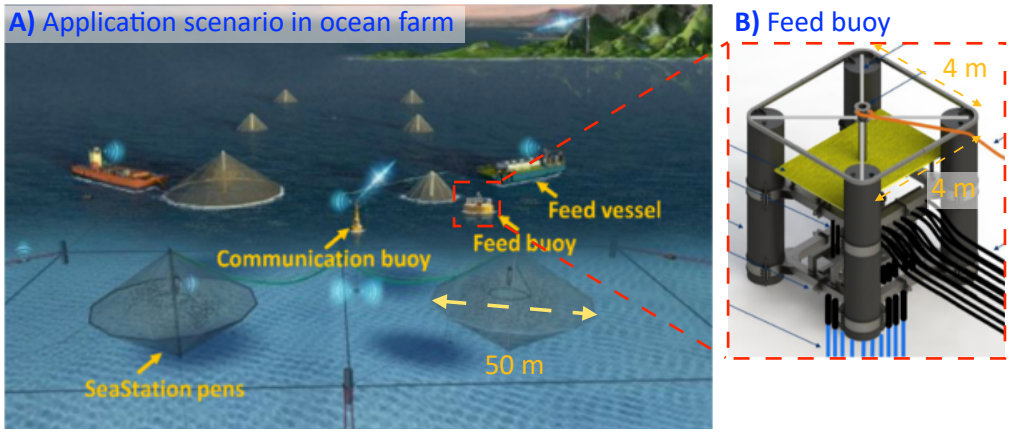

FIGURE 1: ILLUSTRATION OF THE TYPICAL COMPOSITION OF OCEAN FARM.

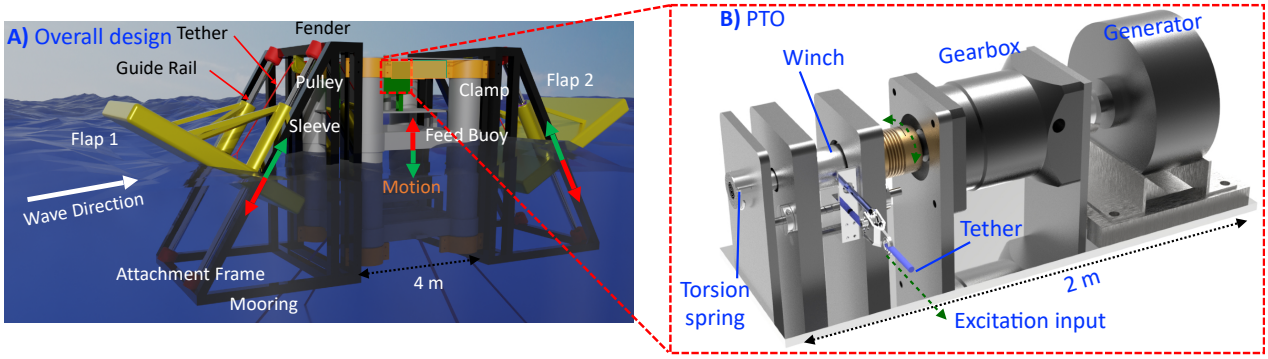

FIGURE 2: CAD DESIGN OF A) THE FLAP-BASED OCEAN WAVE CONVERTER; B) THE WINCH-TETHER-BASED PTO (POWER TAKE OFF SYSTEM).

rotation velocity of the gearbox is $\omega_b = \frac{n}{r}\dot{x}$, where n is gear ratio. The generator can be characterized as the combination of a damping term due to electromagnetic induction and an inertia term due to rotation inertia of the generator rotor. When the generator is engaged with the gearbox, the rotation velocity of the generator is the same as the gearbox output, *i.e.*, $\omega_g = \omega_b$. Hence, the torque produced by the generator is

$$\tau = J_g\dot{\omega}_g + c_g\omega_g = \frac{nJ_g}{r}\ddot{x} + \frac{nk_tk_e}{r(R_i+R_L)}\dot{x} \tag{1}$$

where J_g is the rotational inertia of the generator; c_e is the damping coefficient provided by the generator and $c_e = \frac{k_tk_e}{R_i+R_L}$, where k_e and k_t are the speed constant and torque constant of the generator respectively. R_i and R_L are the internal and external resistance of the generator respectively. The derivation of this equation can be found in [19]. The torque is magnified by the gearbox and converted to translational force on the tether.

$$F = \frac{n\tau}{r} = \frac{n^2J_g}{r^2}\ddot{x} + \frac{n^2k_tk_e}{r^2(R_i+R_L)}\dot{x} \tag{2}$$

The speed constant of the generator can be obtained from the datasheet of the generator or by experiment. It is also noted that even though there is a torsional spring at the end of the winch, its torsional stiffness is designed to be as small as possible, as long as it can retrieve the tether. As a result, it is so small and ignored in the model. It is also noted that all of the winch, the gearbox, the shafts have rotational inertia, however, they are small enough compared with the rotational inertia of the generator rotor, such that it can be ignored. As there is gear contact and bearings, friction is inevitable in the system. The friction torque in the generator is also magnified by the gearbox and becomes more prominent in the system. As a result, a friction torque should be added and in the translational format, which will make the total force

$$F = \frac{n^2J_g}{r^2}\ddot{x} + \frac{n^2k_tk_e}{r^2(R_i+R_L)}\dot{x} + F_r \tag{3}$$

As the tether will be in tension and drive the winch when the input velocity $\dot{x}$ is larger than the rotation speed of the winch. It will be loose when the velocity is smaller. Considering the engage and disengage, the equation of motion becomes

$$\begin{cases} F = \frac{n^2J_g}{r^2}\ddot{x} + \frac{n^2k_tk_e}{r^2(R_i+R_L)}\dot{x} + F_r, \dot{x} > \frac{\omega_g r}{n}, \omega_g = \omega_b \\ F = 0, \dot{x} \leqslant \frac{\omega_g r}{n}, \frac{n^2J_g}{r^2}\dot{\omega}_g + \frac{n^2k_tk_e}{r^2(R_i+R_L)}\omega_g = 0 \end{cases} \tag{4}$$

As a result, the PTO is modeled as an inertia term, a damping term, plus friction in the WEC model.

3.2 WEC dynamics modeling

In order to model the dynamics of the WEC system, the dynamics of the feed buoy, the flaps, and the PTO are considered.

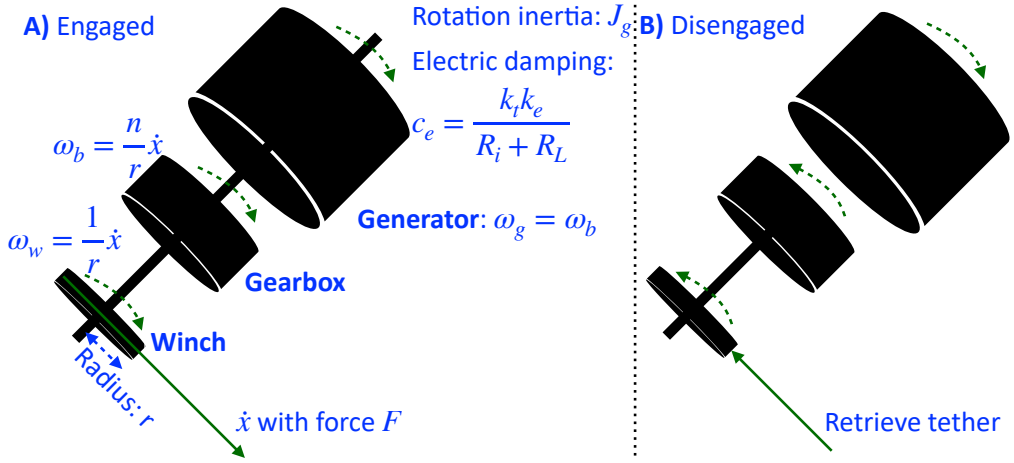

FIGURE 3: PTO LUMPED MODEL.

The feed buoy motion in X, Y, Rx, Ry, Rz directions all are too small and ignored. Only one degree of freedom, *i.e.*, Z direction, is considered. Each flap has one degree of freedom. The tilt angle of the flap$_1$ and flap$_2$ with respect to the feed buoy are both set to θ. The WEC lumped model is shown in Figure 4.

With the lumped model in Figure 4, the equation of motion can be derived from the free body diagram analysis. Since there are 3 degrees of freedom, the equation of motion is more complicated, and the Lagrangian method is used. The potential energy of the whole system is

$$\begin{aligned} V = {} & mgz + m_1 g(z + s_1 \sin\theta) + m_2 g(z + s_2 \sin\theta) \\ & + \frac{1}{2}kz^2 + \frac{1}{2}k_1(z + s_1 \sin\theta)^2 + \frac{1}{2}k_2(z + s_2 \sin\theta)^2 \end{aligned} \tag{5}$$

where m, m_1, m_2 are the mass of the feed buoy, the flap$_1$, the flap$_2$ respectively; m_{a1} and m_{a2} are the added mass of the two flaps respectively; J is the rotational inertial of the generator rotor, c_e is the electrical damping provided by the generator; c_r is the radiation damping induced by the hydrodynamics.

The kinetic energy is

$$\begin{aligned} T = {} & \frac{1}{2}(m + m_a)\dot{z}^2 + \frac{1}{2}(m_1 + m_{1a})[(\dot{z} + \dot{s}_1 \sin\theta)^2 + \dot{s}_1^2 \cos^2\theta] \\ & + \frac{1}{2}(m_2 + m_{2a})[(\dot{z} + \dot{s}_2 \sin\theta)^2 + \dot{s}_2^2 \cos^2\theta] \end{aligned} \tag{6}$$

The Lagrangian is $L = T - V$. The equation of motion with respect to the three degrees of freedom can be obtained by

$$\begin{cases} F_1 = \frac{\partial \frac{\partial L}{\partial \dot{x}}}{\partial t} - \frac{\partial L}{\partial x} \\ F_{ext1} = \frac{\partial \frac{\partial L}{\partial \dot{s}_1}}{\partial t} - \frac{\partial L}{\partial s_1} \\ F_{ext2} = \frac{\partial \frac{\partial L}{\partial \dot{s}_2}}{\partial t} - \frac{\partial L}{\partial s_2} \end{cases} \tag{7}$$

Plug in and add the damping and inertia terms, the equation of motion can be obtained as

$$\begin{cases} F_{ext} = (m + m_a)\ddot{z} + kz + c_r\dot{z} - c_e\dot{s}_1 \sin\theta - J_e\ddot{s}_2 \sin\theta \\ \quad -J_e\ddot{s}_1 \sin\theta - c_e\dot{s}_2 \sin\theta \\ F_{ext1} = (m_1 + m_{1a})(\frac{\ddot{z}}{\sin\theta} + \ddot{s}_1) + k_1(\frac{z}{\sin\theta} + s_1) \\ \quad +c_{r1}(\frac{\dot{z}}{\sin\theta} + \dot{s}_1) + c_e\dot{s}_1 + J_e\ddot{s}_1 \\ F_{ext2} = (m_2 + m_{2a})(\frac{\ddot{z}}{\sin\theta} + \ddot{s}_2) + k_2(\frac{z}{\sin\theta} + s_2) \\ \quad +c_{r2}(\frac{\dot{z}}{\sin\theta} + \dot{s}_2) + c_e\dot{s}_2 + J_e\ddot{s}_2 \end{cases} \tag{8}$$

where $c_e = \frac{n^2 k_t k_e}{r^2(R_i + R_L)}$, and $J_e = \frac{n^2 J_g}{r^2}$. Rearrange and the final equation of motion is

$$\begin{cases} \ddot{z} = \frac{F_{ext} - kz - c_r\dot{z} + c_e\dot{s}_1 \sin\theta + c_e\dot{s}_2 \sin\theta + J_e\ddot{s}_2 \sin\theta + J_e\ddot{s}_1 \sin\theta}{m + m_a} \\ \ddot{s}_1 = \frac{F_{ext1} \sin\theta - k_1(z + s_1 \sin\theta) - c_{r1}(\dot{z} + \dot{s}_1 \sin\theta) - c_e\dot{s}_1 \sin\theta - J_e\ddot{s}_1 \sin\theta}{(m_1 + m_{1a})\sin\theta} - \frac{\ddot{z}}{\sin\theta} \\ \ddot{s}_2 = \frac{F_{ext2} \sin\theta - k_2(z + s_2 \sin\theta) - c_{r2}(\dot{z} + \dot{s}_2 \sin\theta) - c_e\dot{s}_2 \sin\theta - J_e\ddot{s}_2 \sin\theta}{(m_2 + m_{2a})\sin\theta} - \frac{\ddot{z}}{\sin\theta} \end{cases} \tag{9}$$

The system equation of motion when disengaged can also be obtained by getting rid of the corresponding damping and inertia terms in the generator rotor.

3.3 Simulation with ANSYS AQWA

The whole system model is built in ANSYS AQWA, as shown in Figure 3. The physical characteristics were input to AQWA, which includes the dimensions and weight of the WEC. All the added mass, radiation damping, and hydrodynamic forces were calculated by AQWA, and time-domain simulation is carried out with linear wave theory. The local mesh element size is 0.2 meters for the flaps and 0.4 meters for the feed buoy, which is small enough to obtain reliable results. The meshed view of the whole system is shown in Figure 5.

The system responds with excitation from different wave heights and periods are done. Since the optimal power can be obtained from resonance, the resonance in each of the flap angle needs to be obtained by a tuning process. The tuning process is shown in Figure 6.

The resonance frequency of the WEC is obtained to be the same as excitation frequency. The final optimal power output still depends on the optimal damping that is provided by the PTO. The process that obtains the optimal damping is shown in Figure 7.

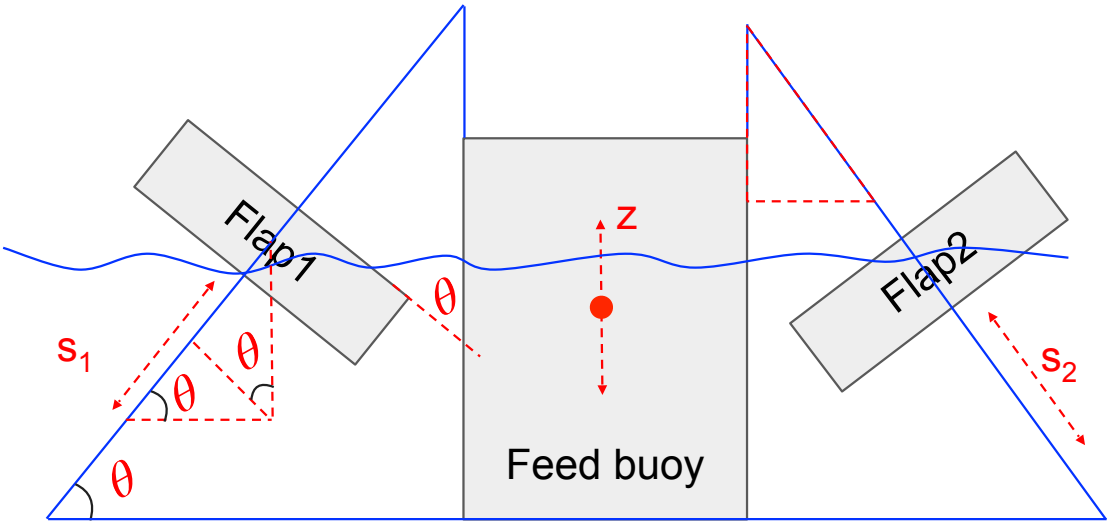

FIGURE 4: WEC LUMPED MODEL WHILE HAVING INTERACTION WITH THE OCEAN WATER.

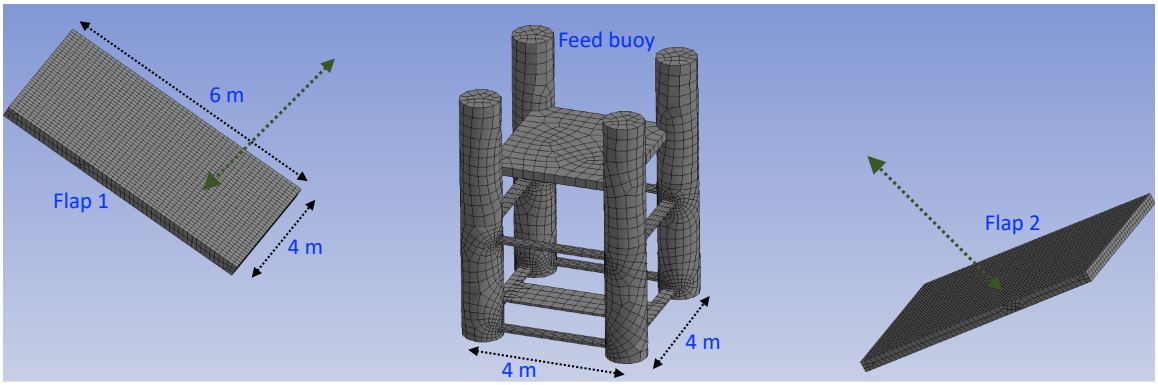

FIGURE 5: MESHED VIEW OF THE WEC.

From the flap angle tuning, it is found that the angle for the optimal power output happens at around 60°. After the tuning process, the optimal power at the optimal flap angle is obtained and shown in Figure 8.

After obtaining optimal thickness, optimal angle, and optimal damping, the optimal power output with excitation at Panama can be obtained and shown in Figure 9.

From Figure 9 , the power output can be obtained with the increase of wave height and wave period. The maximum power that can be obtained is at 9.5 s and 3.0 m wave height. The wave potential can be calculated by

$$P = \frac{\rho g^2}{64\pi} H_{m0}^2 T \tag{10}$$

Apply the ocean water density ρ=1036 kg/m^3, gravity constant g=9.81 N/kg, significant wave height H and wave period T, the power potential and hence the the capture width ratio (CWR) can be obtained gross average CWR is 13%.

TABLE 1: PROTOTYPE PARAMETERS.

Symbol	Parameter explanation	Quantity
n	Gear ratio	3
r	Winch radius	23 mm
J_g	Rotation inertia of rotor	2.6 kgm^2
k_e	Speed constant	0.48 Vs/rad
k_t	Torque constant	0.48 Nms/rad

4. PROTOTYPE AND EXPERIMENTAL EVALUATION

4.1 Prototype

The PTO prototype is fabricated and assembled by the machine shop according to the CAD and shown in Figure 10.

The key parameters are shown in Table 1

As shown in Figure 11, the whole WEC is prototyped and assembled. In the next section, the prototype will be characterized in wave tank settings.

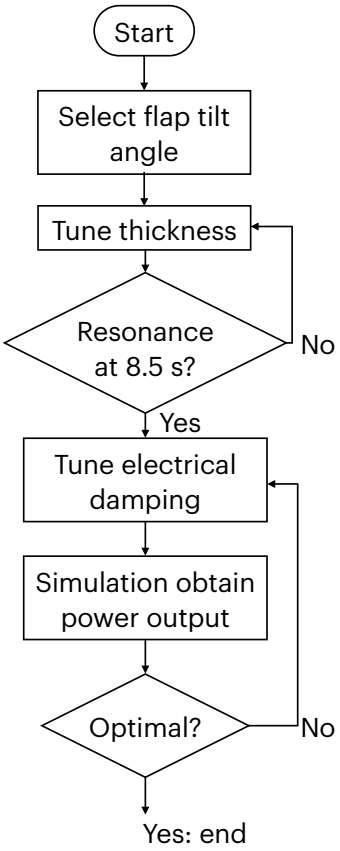

FIGURE 6: SIMULATION PROCEDURE FLOW CHART.

4.2 Characterization of the PTO

In order to evaluate the performance of the winch-based PTO, experiment is set up and shown in Figure 12. Instron is used to provide controlled displacement input. The PTO is clamped on the upper grip and the end of the tether is clamped to the low grip. The relative displacement between the two clamps drives the winch to rotate. The voltage output of the generator is sampled and recorded by a data acquisition system (Coco-80). A load sensor at the end of the upper grip is used to measure the load (force) input to the PTO.

In order to test the PTO system, the Instron was used to provide displacement inputs. First, we applied a triangle wave with 20 mm amplitude, and a frequency of 1 Hz. This was done with no external load on the generator, *i.e.*, the generator has an open circuit. The input, as well as the output is shown in Figure 13.

From the experiment, multiple system parameters can be identified. Since the generator is open circuit, the load at steady state (*i.e.* 0.5-0.7 s in Figure 13) is the friction force, and it is identified as 100 N. With 20 mm and 1 Hz triangle displacement input, the velocity is 0.08 m/s. Convert to rotation by the winch (with a radius of 0.22 m), the rotation velocity is 3.48 rad/s. Magnified by gearbox (3 times), the rotation velocity of the generator is 10.4 rad/s. The voltage output is 5 V. Then the speed constant is identified as 0.48 Vs/rad.

4.3 System performance under sinusoidal and scaled-down ocean excitation input

In order to test the efficiency of the PTO system, the output side of the generator was connected to a 1 Ω load. Then a sinusoidal excitation input with an amplitude of 20 mm and a frequency of 1 Hz is applied. The results of this experiment are shown in Figure 14.

From Figure 14 C, the energy input to the PTO in one cycle can be determined by the enclosed area in the force-displacement loop and is calculated to be 14.1 J. The average power output of the generator is 7.8 W, and thus in one cycle, produces 7.8 J of energy, as a result, the overall efficiency $\eta_{overall}$ can be determined to be 55.3%. Considering the internal resistance 0.5 Ω and external resistor 1Ω, the electrical efficiency $\eta_e$is 66.7%, as $\eta_e = \frac{R_L}{R_i+R_L}$. Since $\eta_{overall} = \eta_e\eta_m$, the mechanical efficiency η_m is calculated as 83%.

Lastly, we ran an experiment with a scaled down irregular wave excitation input and shown in Figure 15. This test was used to analyze if the PTO performed at the same efficiency with both regular and irregular wave inputs. From Figure 15, the overall efficiency is obtained as 55% from this experiment, which is highly similar to that of the 1 Hz sinusoidal excitation test, indicating that there is no PTO loss associated with irregular inputs.

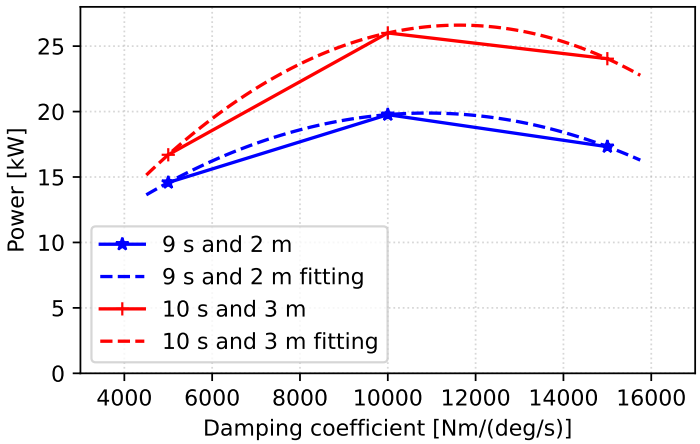

FIGURE 7: POWER OUTPUT OPTIMIZATION OVER ELECTRICAL DAMPING. THE OPTIMAL POWER OUTPUT IS OBTAINED FROM THE MAXIMUM POWER OUTPUT POINT OF THE FITTED CURVE.

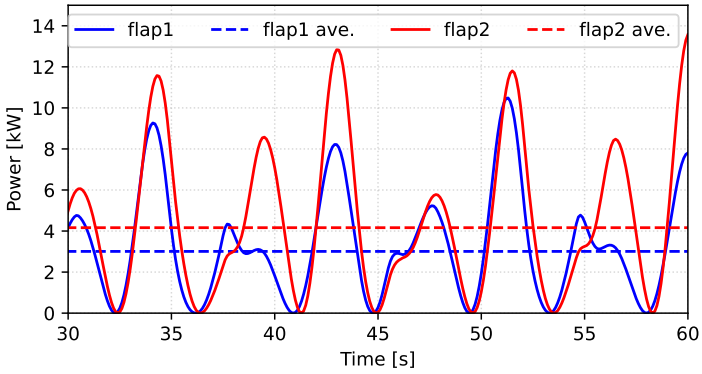

FIGURE 8: THE POWER OUTPUT VS. AVERAGE POWER OUTPUT OF THE TWO FLAPS. THE EXCITATION CONDITION IS 8.5 S WAVE PERIOD AND 1.5 METER WAVE HEIGHT.

4.4 Characterization of the WEC

To characterize the PTO, both free decay test and RAO (Response Amplitude Operators) test were carried out. The flap is set to a position that is off balance and release. The time domain response of the WEC (*i.e.*, the motion of the flaps) are recorded and shown in Figure 16. As shown in Figure 16, the resonance period of the WEC is obtained as 3 s, which according to scale of 1:8 and Froude scaling law, would result in the targeted excitation frequency of 8.5 s.

The system RAO is obtained by having a period sinusoidal excitation wave with 4 s period and 0.1 m height. The results are shown in Figure 17. Considering the excitation wave height of 0.1 m, the RAO of the two flaps are hence obtained as 1.25 and 0.79 respectively.

5. CONCLUSIONS

In this paper, a self-reactive wave energy converter and winch-based PTO is conceived, designed, modeled, simulated, and tested on wave tank. From simulation, a 13% of capture width ratio is achieved. A scaled down PTO is prototyped, and experimentally evaluated. The experimental results found out that the mechanical power is converted to electrical power with an efficiency of 83%. Ocean wave tank test had verified the self-reaction property of the WEC and a good RAO is also obtained. The CWR achieved is still less than idea. Future work should be improving the system performance, building full version prototype and test out in real ocean settings.

REFERENCES

[1] F. FAO, General situation of world fish stocks (2005).

[2] A. O. of the United Nations. Fisheries Department, The State of World Fisheries and Aquaculture, 2000, Vol. 3, Food & Agriculture Org., 2000.

[3] P. T. Jacobson, G. Hagerman, G. Scott, Mapping and assessment of the united states ocean wave energy resource, Tech. rep., Electric Power Research Institute (2011).

[4] T. K. Brekken, A. Von Jouanne, H. Y. Han, Ocean wave energy overview and research at oregon state university, in: 2009 IEEE Power Electronics and Machines in Wind Applications, IEEE, 2009, pp. 1–7.

[5] R. Henderson, Design, simulation, and testing of a novel hydraulic power take-off system for the pelamis wave energy converter, Renewable energy 31 (2) (2006) 271–283.

Power (kW)		Peak Wave Period [s]						
		5.5	6.5	7.5	8.5	9.5	10.5	11.5
Significant Wave Height [m]	0.5	3.20	1.18	0.99				
	1.0		4.20	3.16	2.06			
	1.5			7.28	4.81	4.25		
	2.0			13.19	8.80	7.55		
	2.5				14.49	11.69	8.68	
	3.0					17.21	12.29	
	3.5						16.98	13.78

FIGURE 9: POWER OUTPUT BY THE WEC AT PANAMA AQUACULTURE FARM SITE UNDER DIFFERENT WAVE EXCITATION CONDITIONS. WAVE PERIOD IS PEAK WAVE PERIOD, AND WAVE HEIGHT IS SIGNIFICANT WAVE HEIGHT SINCE IT IS AN IRREGULAR WAVE MATRIX.

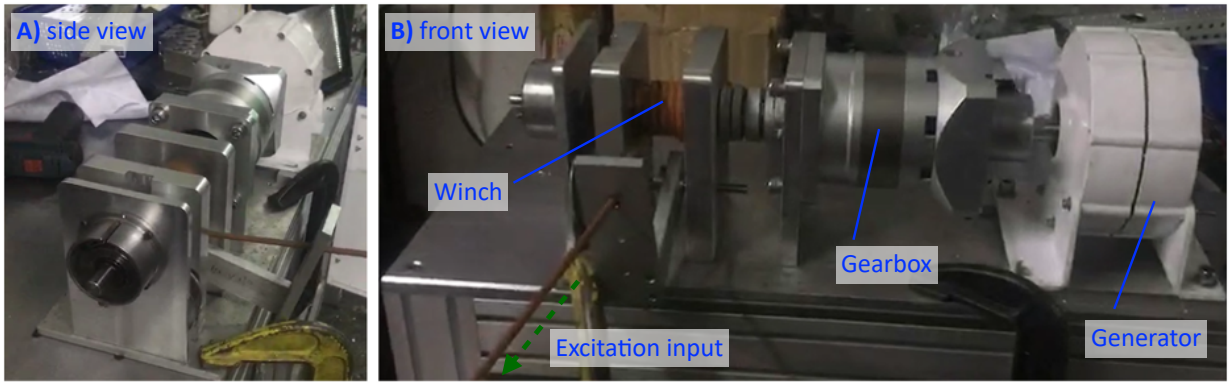

FIGURE 10: PROTOTYPE OF THE WINCH-BASED PTO.

[6] S. H. Salter, Wave power, Nature 249 (5459) (1974) 720–724.

[7] E. Ramudu, Ocean wave energy-driven desalination systems for off-grid coastal communities in developing countries, in: 2011 IEEE Global Humanitarian Technology Conference, IEEE, 2011, pp. 287–289.

[8] A. F. Falcão, J. C. Henriques, Oscillating-water-column wave energy converters and air turbines: A review, Renewable Energy 85 (2016) 1391–1424.

[9] J. Tedd, J. P. Kofoed, Measurements of overtopping flow time series on the wave dragon, wave energy converter, Renewable Energy 34 (3) (2009) 711–717.

[10] M. Lehmann, R. Elandt, M. Shakeri, R. Alam, The wave carpet: development of a submerged pressure differential wave energy converter, in: 30th Symposium on Naval Hydrodynamics, 2014, pp. 2–7.

[11] Y. Kamizuru, Development of hydrostatic drive trains for wave energy converters, Vol. 352, Shaker Herzogenrath, Germany, 2014.

[12] M. Previsic, R. Bedard, G. Hagerman, E1i assessment, offshore wave energy conversion devices, Tech. rep., EPRI WP-004-US–Rev1 (2004).

[13] S. Parmeggiani, J. F. Chozas, A. Pecher, E. Friis-Madsen, H. Sørensen, J. P. Kofoed, Performance assessment of the wave dragon wave energy converter based on the equimar methodology, in: 9th ewtec 2011: Proceedings of the 9th European Wave and Tidal Conference, Southampton, UK, 5th-9th September 2011, University of Southampton, 2011.

[14] J. Cordonnier, F. Gorintin, A. De Cagny, A. Clément, A. Babarit, Searev: Case study of the development of a wave energy converter, Renewable Energy 80 (2015) 40–52.

[15] Y.-H. Yu, Y. Li, K. Hallett, C. Hotimsky, Design and analysis for a floating oscillating surge wave energy converter, in: International Conference on Offshore Mechanics and Arctic Engineering, Vol. 45547, American Society of Mechanical Engineers, 2014, p. V09BT09A048.

[16] P. J. Wooley, M., , . energy on the crest of a wave, New Scientist 65 (1975) 241–243.

[17] R. Yemm, D. Pizer, C. Retzler, R. Henderson, Pelamis: experience from concept to connection, Philosophical Transactions of the Royal Society A: Mathematical, Physical and Engineering Sciences 370 (1959) (2012) 365–380.

[18] S. Salter, D. Jeffrey, J. Taylor, The architecture of nodding duck wave power generators (1976).

[19] M. Liu, W.-C. Tai, L. Zuo, Toward broadband vibration energy harvesting via mechanical motion-rectification induced inertia nonlinearity, Smart Materials and Structures 27 (7) (2018) 075022.

,

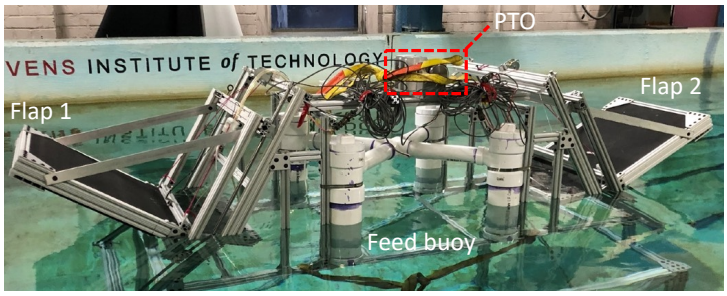

FIGURE 11: THE PROTOTYPE OF THE WEC IN A WAVE TANK SETTING. A FRAME IS USED TO REPRESENT THE FEED BUOY AND THE FLAPS IS INSTALLED ON IT.

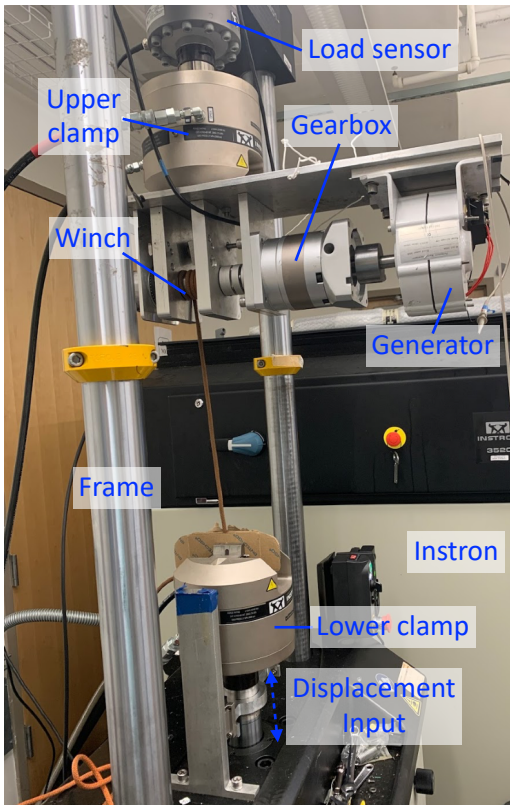

FIGURE 12: SYSTEM CHARACTERIZATION EXPERIMENT SETUP.

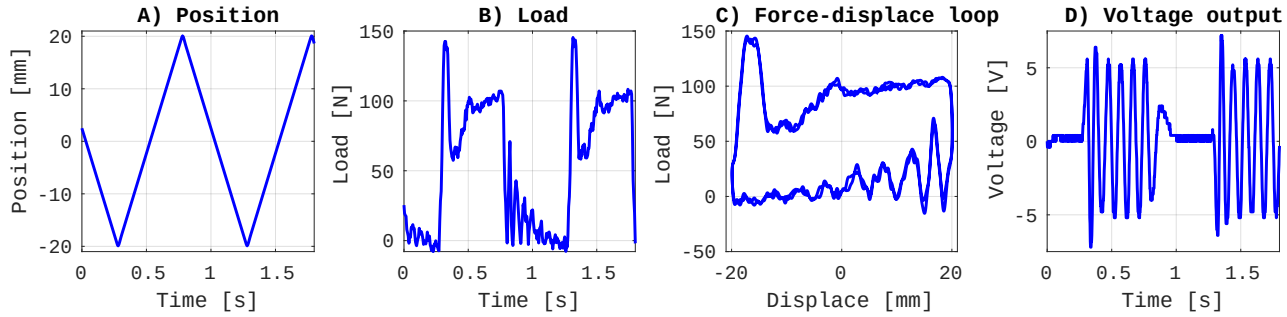

FIGURE 13: EXPERIMENT RESULT WITH TRIANGLE WAVE INPUT. A) PTO POSITION INPUT; B) PTO LOAD OUTPUT; C) FORCE-DISPLACEMENT LOOP OF THE PTO. D) VOLTAGE OUTPUT OF THE GENERATOR.

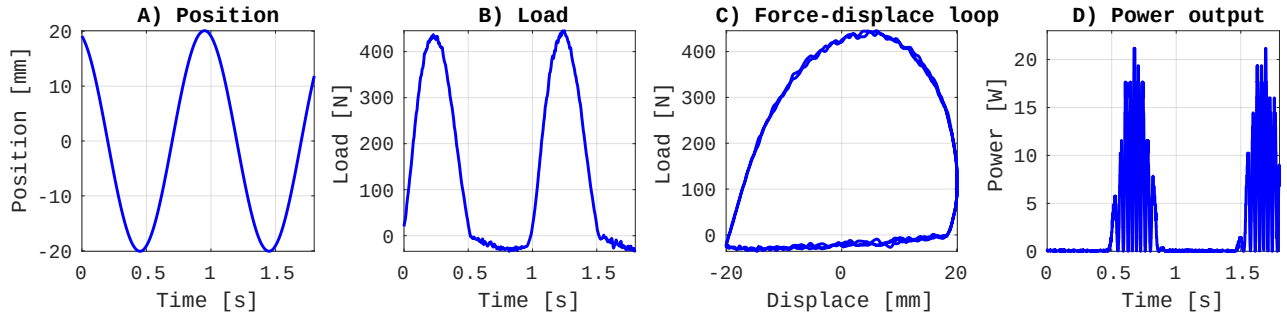

FIGURE 14: EXPERIMENT RESULT WITH TRIANGLE WAVE INPUT. A) PTO POSITION INPUT; B) PTO LOAD INPUT; C) FORCE-DISPLACEMENT LOOP OF THE PTO. D) PTO POWER OUTPUT.

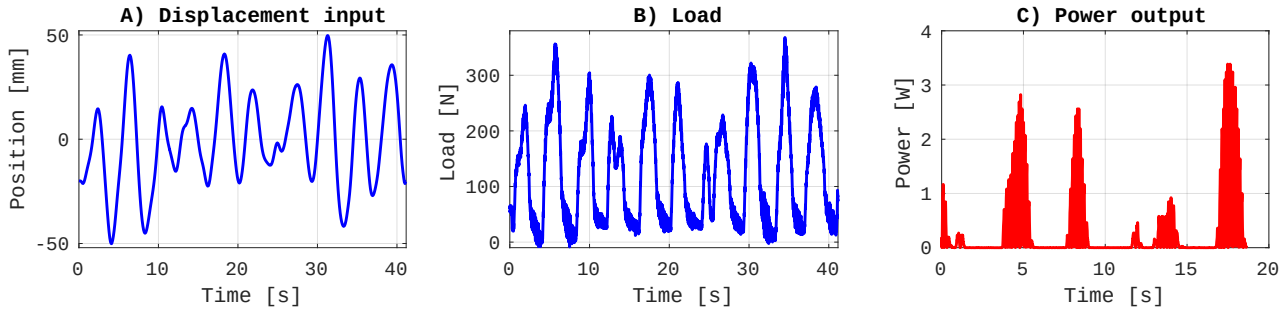

FIGURE 15: EXPERIMENT RESULT WITH TRIANGLE WAVE INPUT. A) PTO POSITION INPUT; B) PTO LOAD INPUT; C) PTO POWER OUTPUT.

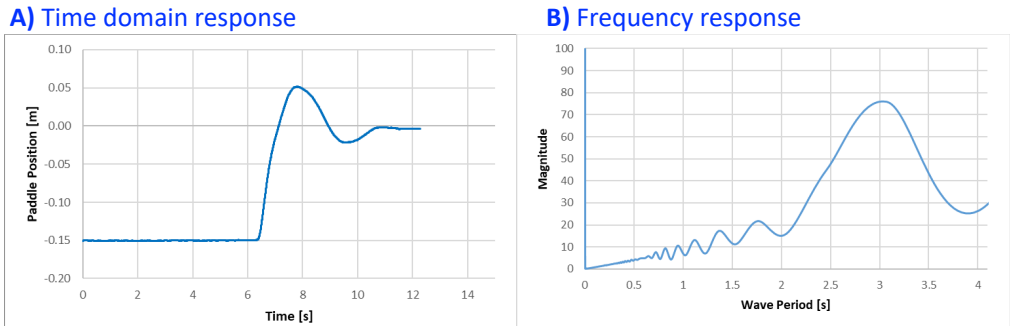

FIGURE 16: FREE DECAY TEST OF THE WEC. A) TIME DOMAIN RESULTS; B) FREQUENCY DOMAIN RESULTS.

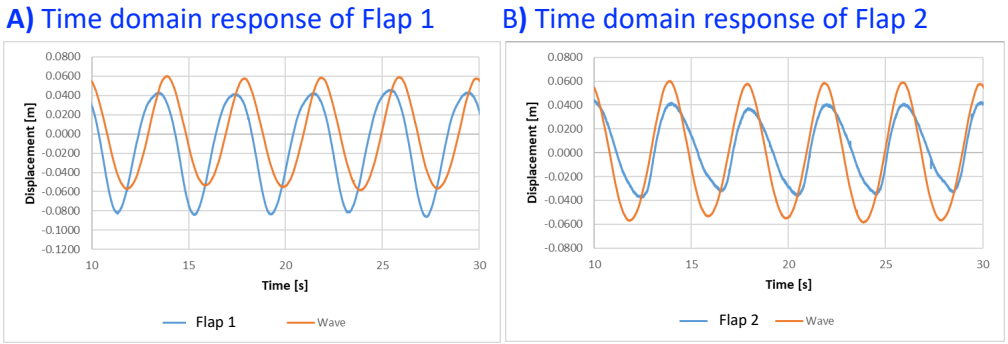

FIGURE 17: RAO TEST OF THE WEC. BOTH THE RESPONSE FLAP 1 AND FLAP 2 OF THE WEC ARE OBTAINED.